Magnetism in dehydrogenated armchair graphene nanoribbon

Magnetism in Dehydrogenated Armchair Graphene Nanoribbon

Keisuke Sawada[1], Fumiyuki Ishii[2], and Mineo Saito[2,3]

[1]*Division of Mathematical and Physical Science, Graduate School of Natural Science and Technology, Kanazawa University, Kakuma, Kanazawa 920-1192, Japan*

[2]*Faculty of Mathematics and Physics, Institute of Science and Engineering, Kanazawa University, Kanazawa, 920-1192, Japan*

[3]*Collaborative Research Center for Frontier Simulation Software for Industrial Science, Institute of Industrial Science, University of Tokyo, 4-6-1 Komaba, Meguro-ku, Tokyo 153-8503, Japan*

Although the zigzag graphene nanoribbon attracts scientific interest because of its magnetic properties, the study of the magnetism of the armchair graphene nanoribbons (AGNRs) is insufficient. By using first-principles calculations, we find that the magnetic state of dehydrogenated AGNRs is stable in a wide range of electron doping. The spin polarization originates from the localized edge state around the Brillouin zone boundary. In the case of field effect transistor doping, some of the electrons injected into indirect-gap AGNRs induce half-metallicity and heavily doped direct-gap AGNRs are antiferromagnetic. We also find that nitrogen doping produces ferromagnetic insulators and half-metals.

KEYWORDS: armchair graphene nanoribbon, first-principles calculation, magnetism, carrier doping, chemical doping

1. Introduction

Recently, graphene-based materials have attracted much attention owing to the successful fabrication of graphenes.[1] Graphenes have many useful properties for spintronics applications. For an example, spin transport has been experimentally observed by using graphene layers[2–4] and a half-metallic property has been theoretically predicted for nanographenes.[5–7]

There are two types of graphene nanoribbons (GNRs); one is the armchair GNR (AGNR) and the other is the zigzag GNR (ZGNR). ZGNRs have attracted scientific interest since the magnetic properties of graphenes are expected to originate from the edge states. Fujita and coworkers clarified that hydrogenated ZGNRs have flat electron bands and the antiferromagnetic (AFM) ground state, which is accompanied by the *anti-parallel interedge spin* (APIES) configuration of the two ferromagnetic (FM) chains located at both edges.[8,9] First-principles calculations confirmed that both hydrogenated and dehydrogenated ZGNRs have the AFM ground state.[10–12] A recent study revealed that doping leads to the noncollinear magnetic state and the *parallel interedge spin* (PIES) state accompanied by the parallel configuration of the two FM chains located at both edges.[13] On the other hand, hydrogenated and dehydrogenated AGNRs have the nonmagnetic (NM) ground state.[14] It was theoretically considered that *heavily doped hydrogenated* AGNRs have the FM ground state.[15]

In this study, we perform first-principles density functional calculations on *dehydrogenated* AGNRs. Strong bonds are formed at the edges; thus, the electronic structure of the dehydrogenated AGNR is different from that of the hydrogenated AGNR. We find that the magnetic state of AGNRs is stable in a *wide range of electron doping*. This magnetism originates from conduction bands having σ characters. In the case of field effect transistor doping, some of the electrons injected into indirect-gap AGNRs induce half-metallicity and heavily doped direct-gap AGNRs are AFM. We also find that N doping leads to FM properties.

2. First-Principles Methods

We perform first-principles electronic-structure calculations based on the density functional theory. The exchange correlation potential is based on the spin-polarized generalized gradient approximation[16] and norm-conserving pseudopotentials[17] with a partial core correction[18] are used. Wavefunctions are expanded by a linear combination of multiple pseudo atomic orbitals:[19,20] two s-orbitals and two p-orbitals of the C atom are used. We confirm that the convergence of the total energy for the basis set is within 0.6 meV/cell. 60 k points are used in the Brillouin zone integration; the total energy varies within 0.01 meV/cell when 120 k points are used. We perform geometry optimization for each spin configuration. All the calculations are performed by using the OPENMX code.[21]

3. Results and Discussion

3.1 Nondoped dehydrogenated AGNR

First, we study the geometry of the nondoped dehydrogenated AGNR in the case of N_w = 7, where N_w denotes the ribbon width (Fig. 1). We start self-consistent calculations by determining the initial magnetic configurations of the PIES [Fig. 2(a)] and APIES [Fig. 2(b)] states, and find that the final magnetic state is NM. These results indicate that the PIES and APIES states are unstable and only the NM state is stable. The bond length between the edge C atoms is 1.27 Å, which is smaller than that of pristine graphene (1.42 Å). This short bond corresponds to a triple bond and induces a large indirect band gap [Fig. 3(a)]. As a result, this AGNR is an NM insulator. The valence band top is located at the Γ-point, whereas the conduction band bottom is located at the X-point (X = π/a).

The wavefunctions of the lowest and second-lowest unoccupied states at the X-point are shown in Figs. 3(b) and 3(c), respectively. The signs at the two edges are the same [different] in Fig. 3(b) [Fig. 3(c)]. As a result, the former wavefunction has a 0.17 eV lower energy than the latter wavefunction. The dispersions of the two bands located near the X-point are small; thus, electron doping is expected to induce magnetism.

Since triple bonds are formed at the edges, the electronic structure of the dehydrogenated AGNR is different from that of the hydrogenated AGNR. The lowest conduction band consists of σ orbitals, whereas the magnetism of the doped hydrogenated AGNR originates from π orbitals.[15]

3.2 Electron-doped dehydrogenated AGNR

Here, we study the electron-doped AGNR by using the Fermi level shift (FLS) method: When the electron is injected into the unit cell, we introduce a uniform positive background charge to make the system neutral. We first investigate the magnetic state of the AGNR when the electron concentration x is 0.2 e/cell. Geometry optimization is performed and the bond length of the edge C atoms is found to be 1.28 Å. This bond length is slightly larger than that in the nondoped case (1.27 Å) owing to the fact that electrons occupy the lowest antibonding character band [Fig. 3(b)]. In the PIES state, the parallel configuration of the two FM chains located at both edges [Fig. 2(a)] is more stable than that in the NM state. The difference between the total energies of the PIES and NM states is 2.4 meV/cell. As shown by the band structure and density of states in Fig. 4, the most stable PIES state has a *half-metallic* property. This spin polarization originates from the localized edge state around the X-point, as shown in Fig. 3(b) or 3(c). Such edge-localized spin polarization reminds us of the flat-band ferromagnetism originating from the localized edge state in the ZGNR.

We examine various AFM states and find that they are unstable. The APIES state shown in Fig. 2(b) and the AFM chains at the edges are unstable. By using a double-size cell, we calculate the chain of the AFM configuration of the FM dimers and find that this state is

also unstable. We study the electron carrier concentration dependence of magnetic states in the AGNR. Figure 5(a) shows the relative total energies of the PIES, APIES, and NM states. When $x = 0.1$ and 0.2 e/cell, the PIES state is the ground state and the NM and APIES states are metastable and unstable, respectively. In the region where 0.3 e/cell $\leq x \leq$ 1.0 e/cell, the APIES state has the lowest energy and the NM and PIES states are metastable. Figure 5(b) shows that the total spin moment of the PIES state mainly originates from the edge C atoms.

In Fig. 6, we show the band structures of the metastable PIES state when $x = 0.4$ and 0.7 e/cell. The difference between the energies of the majority and minority spin conduction bands at the X-point increases when x increases from 0.2 e/cell (Fig. 4) to 0.7 e/cell (Fig. 6). Therefore, even when x is large (0.3 e/cell $\leq x \leq$ 0.9 e/cell), all the injected electrons still occupy the two majority spin bands. As a result, the system shows a half-metallic property when 0.1 e/cell $\leq x \leq$ 0.9 e/cell. However, when $x = 1.0$ e/cell, the minority spin band is partially occupied; thus, the system is not half-metal. As shown in Fig. 5(b), the total spin moment is proportional to x when 0.1 e/cell $\leq x \leq$ 0.9 e/cell, which indicates that this system is a half-metal.

In the APIES state, the two spin bands are degenerated (Fig. 6). In the case of 0.3 e/cell $\leq x \leq$ 1.0 e/cell, the injected electrons partially occupy the lowest conduction band whose wavefunctions have the same phase at the two edges. This is in contrast to the PIES state: The injected electrons occupy the two majority-spin bands whose wavefunctions have the same and opposite phases when 0.3 e/cell $\leq x \leq$ 1.0 e/cell. This occupation of the second-lowest conduction band is expected to increase the total energy of the PIES state.

As mentioned above, when $x \geq 0.3$ e/cell, the APIES state is the ground state and the PIES state has a higher energy than the APIES one. Even in this case, the ground PIES state is expected to be achieved by the following two ways. If magnetic fields whose directions are the same at both edges are introduced, the PIES state becomes the ground state, as was discussed in a previous study.[22] The magnetic field converting the energetical order ranges from 67 to 73 T, which is estimated from the total energy difference between the PIES and APIES states ($x = 0.4$ - 0.8 e/cell). We propose another method. Ferromagnets, such as Fe, Co, and Ni, are used to flip the edge spin in electron-doped AGNRs: Ferromagnets are located on both sides of AGNRs. If the exchange interaction between the edge atoms and the ferromagnet is larger than that between carbon atoms at both edges, the magnetic state of AGNRs can be controlled by the spin direction of ferromagnets: the PIES state can be achieved when ferromagnets on both sides have the same spin direction.

Here, we examine the stability of the PIES state in highly doped AGNRs. When $x = 0.1$ e/cell and 0.2 e/cell, the PIES state is the ground state and the difference between the energies of the PIES and NM states is small (1.3 and 2.4 meV/cell, respectively). On the other hand, when $x = 0.7$ e/cell, the difference between the total energies of the PIES and NM states

increase (17.3 meV/cell), though the APIES state is the ground state. Therefore, if we can achieve the situation where the PIES state has a much lower energy than the APIES state by using the methods mentioned above, the system is expected to be thermally stable.

As mentioned above, we found that half-metallicity can be achieved when an electron is injected into the lowest conduction band at the X-point. Here, we discuss the relationship between the ribbon width (N_w) and the energetical order of the Γ- and X-points. As shown in Fig. 7, the energy of the lowest conduction band at the X-point measured from that at the Γ-point tends to increase with N_w. The difference between the energies at the Γ- and X-points when $N_w = 3n + 1$ tends to be higher than those when $N_w = 3n$ and $3n + 2$. This three-time cycle is expected to originate from the quantum confinement, as was discussed in the case of hydrogenated AGNRs.[23] We find that the conduction-band bottom is located at the X-point when N_w = 4, 5, 7, and 10. In the case of N_w = 7, the system is made half-metallic by a certain amount of electron doping, as was mentioned (Fig. 5). In the cases of N_w = 4, 5, and 10, we also find that half-metallicity is achieved by doping.

When the energy level of the Γ-point of the lowest conduction band is lower than that of the X-point, the levels near the X-point are not occupied in the case of lightly electron doped AGNR; therefore, the system is found to be NM. However, heavy electron doping leads to the occupation of the lowest conduction band near the X-point and leads to a magnetic state: we examine the direct-gap AGNRs whose N_w is up to 16 and confirm that heavy electron doping induces the APIES ground state.

3.3 Nitrogen-doped dehydrogenated AGNR

Thus far, we studied the electron-doped AGNR by using the FLS method. The doping is expected to be possible by using the field effect transistor (FET) method. Here, we demonstrate that chemical doping can also be performed, as was discussed in a previous study on the ZGNR.[13] It was reported that substitutional boron impurities induce p-type carbon nanotubes[24,25] and n-type graphene is formed by nitrogen impurities.[26] We here study the N-substituted impurities. In the AGNR (N_w = 7), nitrogen atoms are located at the central part in the super cell that includes 140 host atom sites [Figs. 8(a), 8(c), and 8(e)]. We optimize the geometry and find that the substituted atoms are located on the graphene plane. We find that the PIES state is the ground state, the NM sate is metastable, and *the APIES state is unstable*. The difference between the total energies of the NM and PIES states is shown in Table I. When x is small (0.1 - 0.3 e/cell), the system is an FM insulator. As shown in Figs. 8(a), 8(c), and 8(e), the spin density is localized in the edge region, which is near the nitrogen atoms. This is due to the fact that electrons feel the attractive potential from the nitrogen atom. This localization reduces the band dispersion, and then, the systems are insulators [Figs. 8(b) and 8(d)]. As x increases, the spin densities become delocalized; thus, the band dispersions are large [Fig. 8(f)]. As a result, when $x = 0.4$ and 0.5 e/cell, the systems

are half-metals.

As shown in Table I, the difference between the total energies of the PIES and NM states in the case of chemical doping is larger than that in the case of FET doping. Moreover, since there are no minority spin bands around the Fermi level in the nitrogen-doped half-metallic AGNR as shown in Fig. 8(f), the half-metallic property is thermally robust. Therefore, it is considered that chemical doping is more favorable than FET doping.

4. Summary

We have performed density-functional calculations on dehydrogenated AGNRs. Although dehydrogenated AGNRs are considered to be irrelevant to magnetism, we find that the magnetic state of AGNRs is stable in a wide range of electron doping. The spin polarization originates from the localized edge state around the Brillouin zone boundary.

We studied doped AGNRs by using the FLS method calculations, which are expected to correspond to those in the case of FET doping. When $N_w = 7$, the PIES state is the ground state when $x = 0.1$ and 0.2 e/cell. This PIES state is found to have half-metallic characters. The APIES state is the ground state when 0.3 e/cell $\leq x \leq$ 1.0 e/cell. The metastable PIES state when 0.3 e/cell $\leq x \leq$ 1.0 e/cell is expected to be the most stable when the magnetic field is introduced or the ferromagnets at both edges are introduced. We found that electron-doped AGNRs are half-metals when $N_w = 4$, 5, 7, and 10, and the APIES state of AGNRs, whose N_w is up to 16, is induced by heavy electron doping.

We also studied N doping. When $N_w = 7$, the PIES state is the most stable and the APIES state is unstable. When 0.1 e/cell $\leq x \leq$ 0.3 e/cell, the system is an *FM insulator* and is expected to be useful for spintronics applications. When $x = 0.4$ and 0.5 e/cell, the system is a half-metal, which is more stable than that in the case of FET doping.

The armchair edges of graphenes are often experimentally observed compared with the zigzag edges of graphenes owing to the fact that the former edges are energetically favorable.[14,27] The dehydrogenation of AGNRs can be achieved by elevating temperature, and dehydrogenated AGNRs are very stable since triple bonds are formed at the edges.[14,27–30] Therefore, electron-doped dehydrogenated AGNRs are expected to be suitable for nanospintronics applications.

Acknowledgments

This work was partly supported by Grants-in-Aid for Scientific Research (Nos. 21560030 and 22016003) from the JSPS and by the Next Generation Super Computing Project, Nanoscience Program, MEXT, Japan and the RISS project in the IT program of MEXT. One of the authors (K. S.) thanks the JSPS for the financial support (No. 21-2252). The computations in this research have been performed using the AIST Super Cluster facility at Tsukuba, the supercomputers at the ISSP, University of Tokyo, the RCCS, Okazaki National

Institute, and the IMR, Tohoku University.

References

1) K. S. Novoselov, A. K. Geim, S. V. Morozov, D. Jiang, Y. Zhang, S. V. Dubonos, I. V. Grigorieva, and A. A. Firsov: Science **306** (2004) 666.
2) M. Ohishi, M. Shiraishi, R. Nouchi, T. Nozaki, T. Shinjo, and Y. Suzuki: Jpn. J. Appl. Phys. **46** (2007) L605.
3) N. Tombros, C. Jozsa, M. Popinciuc, H. T. Jonkman, and B. J. van Wees: Nature **448** (2007) 571.
4) M. Nishioka and A. M. Goldman: Appl. Phys. Lett. **90** (2007) 252505.
5) Y. Son, M. L. Cohen, and S. G. Louie: Nature **444** (2006) 347.
6) E. Kan, Z. Li, J. Yang, and J. G. Hou: J. Am. Chem. Soc. **130** (2008) 4224.
7) O. Hod, V. Barone, and G. E. Scuseria: Phys. Rev. B **77** (2008) 035411.
8) M. Fujita, K. Wakabayashi, K. Nakada, and K. Kusakabe: J. Phys. Soc. Jpn. **65** (1996) 1920.
9) K. Nakada, M. Fujita, G. Dresselhaus, and M. S. Dresselhaus: Phys. Rev. B **54** (1996) 17954.
10) H.Lee, N. Park, Y. Son, S. Han, and J. Yu: Chem. Phys. Lett. **398** (2004) 207.
11) H. Lee, Y. Son, N. Park, S. Han, and J. Yu: Phys. Rev. B **72** (2005) 174431.
12) D. Jiang, B. G. Sumpter, and S. Dai: J. Chem. Phys. **126** (2007) 134701.
13) K. Sawada, F. Ishii, M. Saito, S. Okada, and T. Kawai: Nano Lett. **9** (2009) 269.
14) S. Okada: Phys. Rev. B **77** (2008) 041408(R).
15) H. Lin, T. Hikihara, H. Jeng, B. Huang, C. Mou, and X. Hu: Phys. Rev. B **79** (2009) 035405.
16) J. P. Perdew, K. Burke, and M. Ernzerhof: Phys. Rev. Lett. **77** (1996) 3865.
17) N. Troullier and J. L. Martins: Phys. Rev. B **43** (1991) 1993.
18) S. G. Louie, S. Froyen, and M. L. Cohen: Phys. Rev. B **26** (1982) 1738.
19) T. Ozaki: Phys. Rev. B **67** (2003) 155108.
20) T. Ozaki and H. Kino: Phys. Rev. B **69** (2004) 195113.
21) T. Ozaki, H. Kino, J. Yu, M. J. Han, N. Kobayashi, M. Ohfuti, F. Ishii, T. Ohwaki, H. Weng, and K. Terakura: available from (http://www.openmx-square.org/).
22) K. Sawada, F. Ishii, and M. Saito: Appl. Phys. Express **1** (2008) 064004.
23) Y. Son, M. L. Cohen, and S. G. Louie: Phys. Rev. Lett. **97** (2006) 216803.
24) K. McGuire, N. Gothard, P. L. Gai, M. S. Dresselhaus, G. Sumanasekera, and A. M. Rao: Carbon **43** (2005) 219.
25) N. Murata, J. Haruyama, J. Reppert, A. M. Rao, T. Koretsune, S. Saito, M. Matsudaira, and Y. Yagi: Phys. Rev. Lett. **101** (2008) 027002.
26) X. Wang, X. Li, L. Zhang, Y. Yoon, P. K. Weber, H. Wang, J. Guo, and H. Dai: Science **324** (2009) 768.
27) Y. Kobayashi, K. Fukui, T. Enoki, K. Kusakabe, and Y. Kaburagi: Phys. Rev. B **71** (2005) 193406.
28) Y. Lee, S. Kim, and D. Tomanek: Phys. Rev. Lett. **78** (1997) 2393.
29) T. Kawai, Y. Miyamoto, O. Sugino, and Y. Koga: Phys. Rev. B **62** (2000) R16349.
30) L. R. Radovic and B. Bockrath: J. Am. Chem. Soc. **127** (2005) 5917.

Fig. 1. (Color online) Lattice structures of AGNR. The rectangle with solid lines is the unit cell and a is the lattice constant. N_w is the width of the AGNR.

Fig. 2. (Color online) Magnetic structures of the dehydrogenated AGNR. (a) and (b) show the PIES and APIES states, respectively. The arrows represent relative spin directions between different sites. (The absolute spin directions are not determined in the present calculation since we neglect the spin-orbit interaction.)

Fig. 3. (Color online) Electronic structures of the dehydrogenated AGNR. (a) shows the band structure of the NM state. The Fermi level is set to be zero. (b) and (c) show the lowest and second-lowest unoccupied molecular orbitals at the X-point, respectively. The red (dark) and blue (bright) isosurfaces indicate the positive and negative amplitudes of the wavefunctions, respectively. The absolute isovalues are 0.075/Bohr$^{3/2}$.

Fig. 4. (Color online) Band structure (a) and density of states (b) of the PIES state when $x = 0.2$ e/cell. The solid and dashed lines denote the majority and minority spin states, respectively. The Fermi level is set to be zero.

Fig. 5. (Color online) (a) Total energy measured from that of the NM state as a function of x. Circles and triangles denote the PIES and APIES states, respectively. (b) Total spin moment (circles) and the sum of spin moments of edge C atoms (triangles) for the PIES state as a function of x.

Fig. 6. (Color online) Band structures of the (a) PIES and (b) APIES states when $x = 0.4$ e/cell, and the (c) PIES and (d) APIES states when $x = 0.7$ e/cell. The solid and dashed lines in (a) and (c) denote the majority and minority spin states, respectively. The Fermi level is set to be zero.

Fig. 7. (Color online) Difference between the lowest conduction-band energies at the Γ and X points as a function of N_w.

Fig. 8. (Color online) Spin densities and band structures of the PIES state in the nitrogen-doped AGNR. (a), (c), and (e) show the spin density when $x = 0.1$, 0.3, and 0.5 e/cell, respectively. The red (dark) and blue (bright) isosurfaces indicate the majority and minority spins, respectively. The isovalues are 0.0005 e/Bohr^3. (b), (d), and (f) show the band structures when $x = 0.1$, 0.3, and 0.5 e/cell, respectively. The solid and dashed lines denote the majority and minority spin states, respectively. The Fermi levels are set to be zero. X$' = \pi/10$a.

Table I. Total energy difference between the NM and PIES states [$\Delta E = E_{\rm PIES}$ - $E_{\rm NM}$ (meV/cell)] as a function of electron carrier concentrations x. The calculated results in the cases of the chemical doping (Chem) and Fermi-level shift (FLS) are tabulated. I and M denote the FM insulator and half-metal, respectively.

	ΔE (meV/cell)	
x (e/cell)	Chem	FLS
0.1	-4.9 (I)	-1.3 (M)
0.2	-7.8 (I)	-2.4 (M)
0.3	-5.0 (I)	-0.6 (M)
0.4	-6.6 (M)	-1.7 (M)
0.5	-5.9 (M)	-7.9 (M)

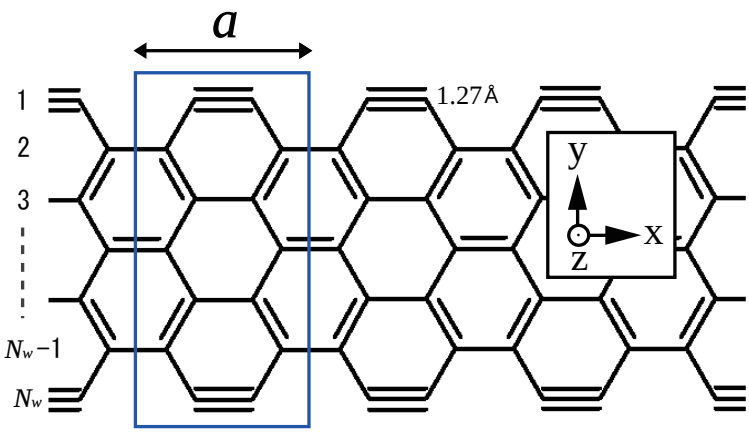

Fig. 1

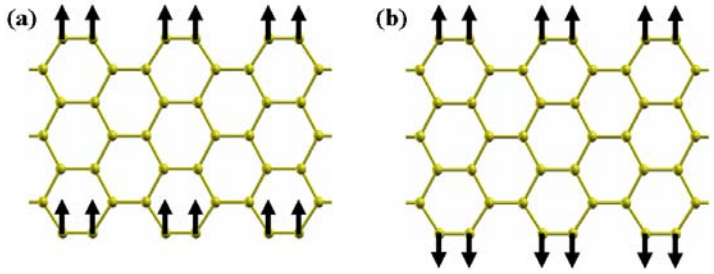

Fig. 2

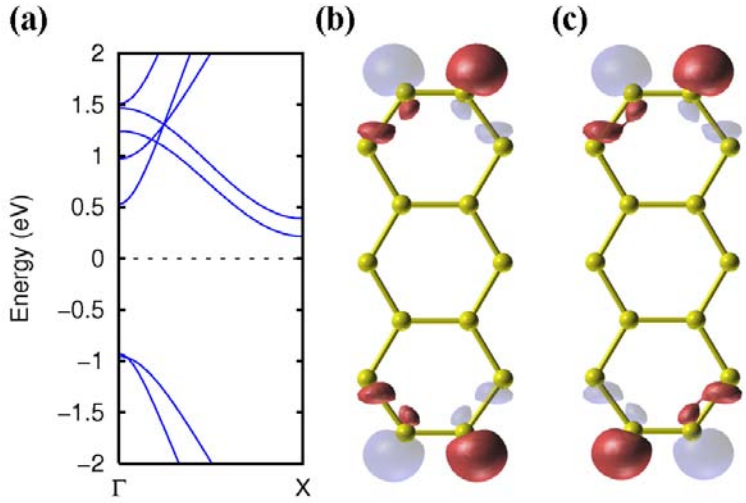

Fig. 3

Fig. 4

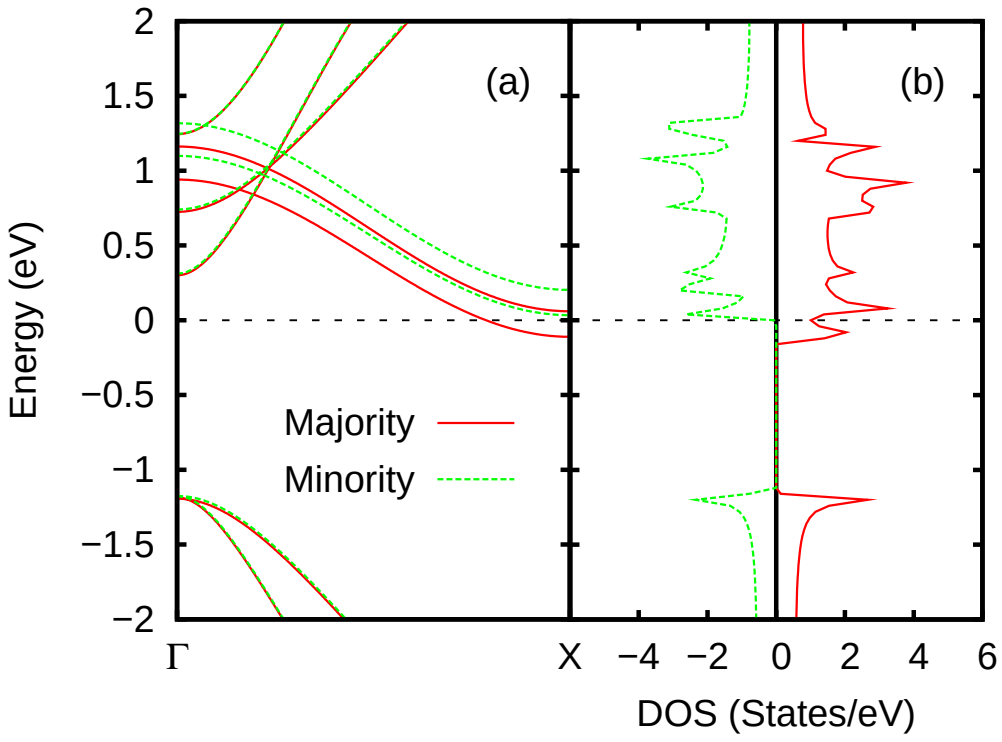
Energy (eV)
2
1.5
1
0.5
0
−0.5
−1
−1.5
−2
Γ
X
(a)
(b)
Majority
Minority
−4
−2
0
2
4
6
DOS (States/eV)

Fig. 5

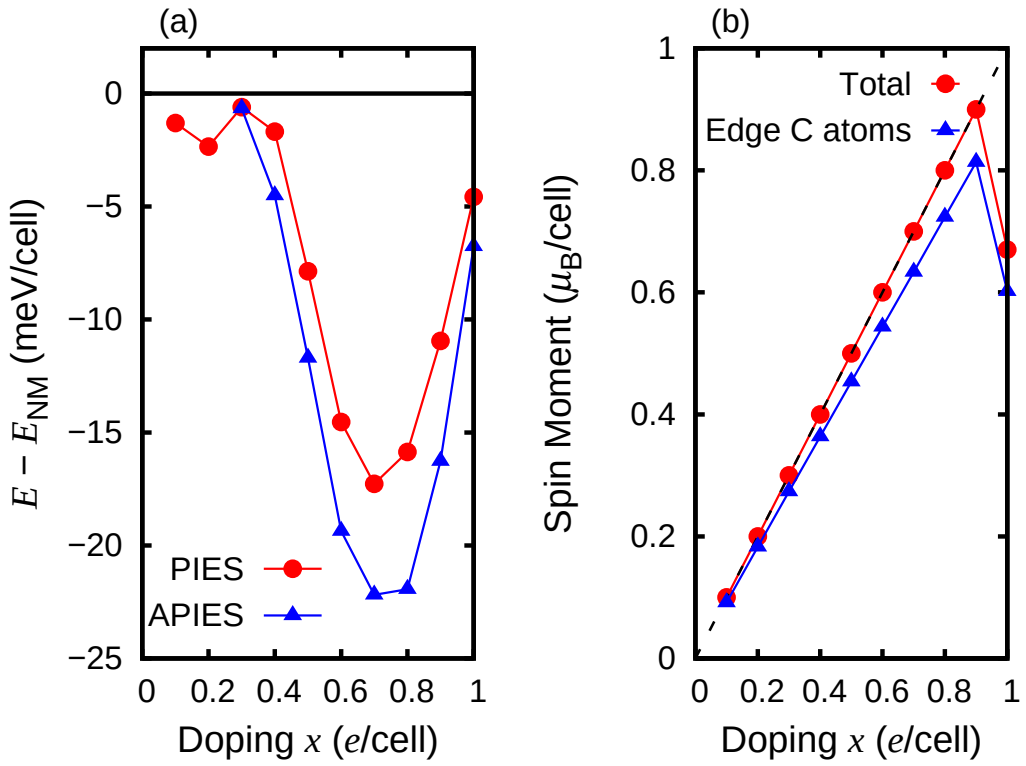
(a)
0
−5
−10
−15
−20
−25
$E - E_{NM}$ (meV/cell)
PIES
APIES
0 0.2 0.4 0.6 0.8 1
Doping x (e/cell)
(b)
1
0.8
0.6
0.4
0.2
0
Spin Moment (μ_B/cell)
Total
Edge C atoms
0 0.2 0.4 0.6 0.8 1
Doping x (e/cell)

Fig. 6

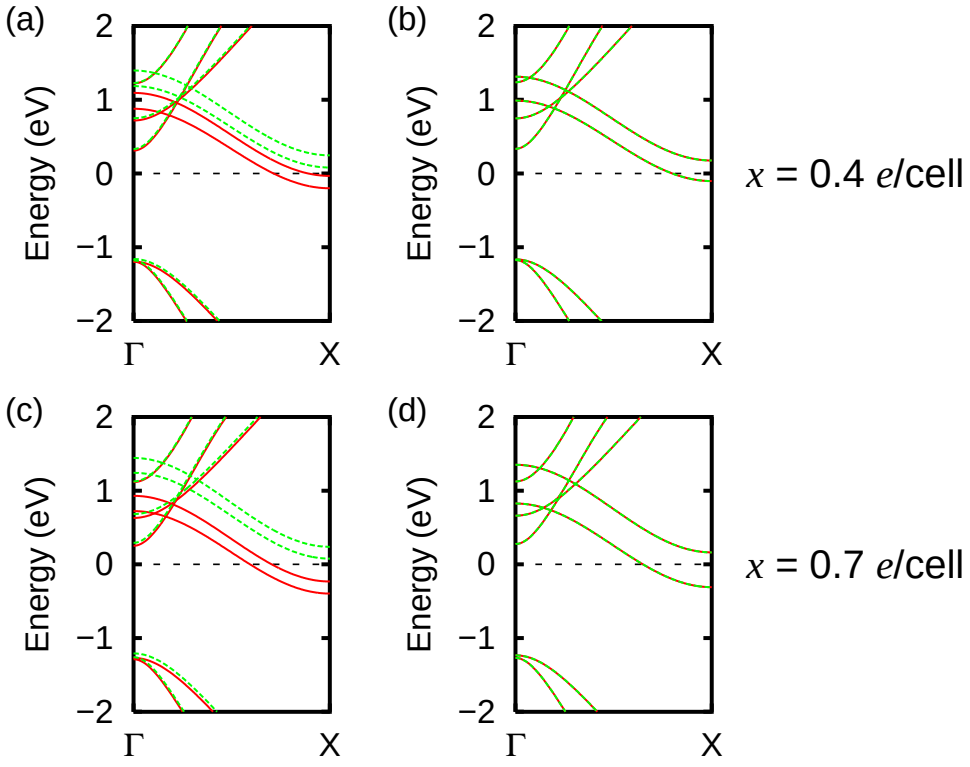

Fig. 7

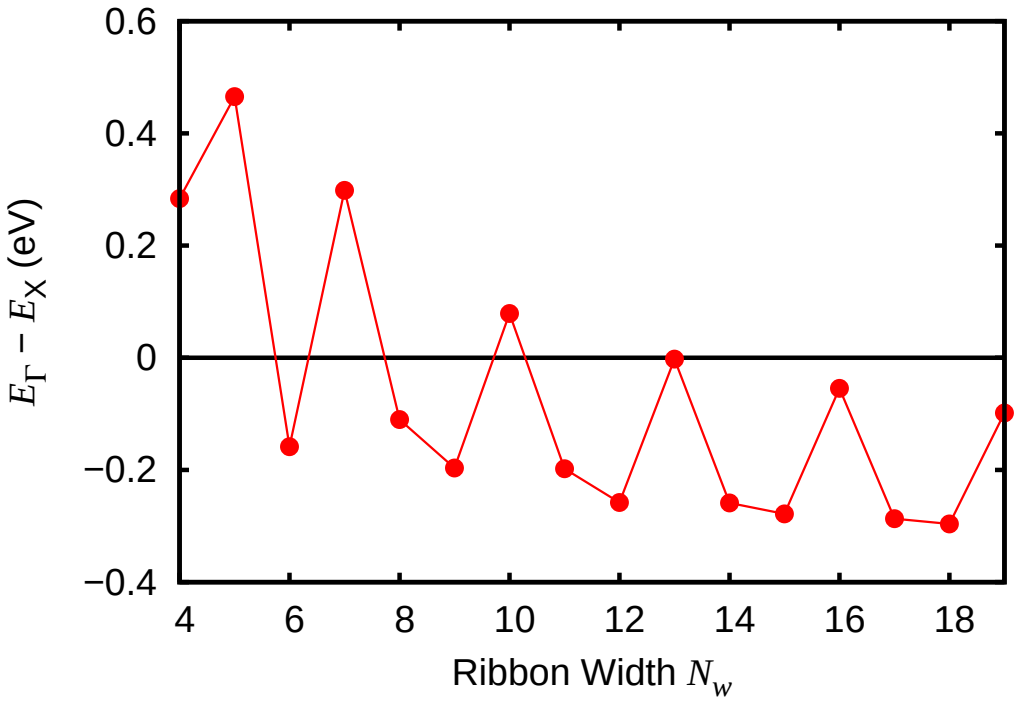

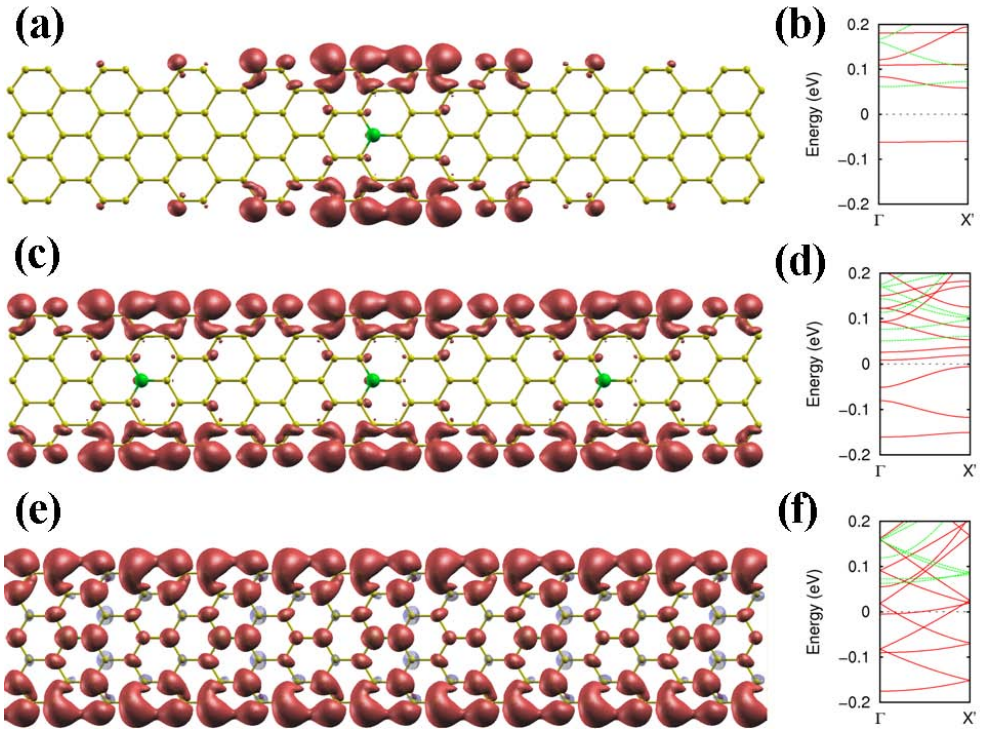

Fig. 8